

## X-ray spectroscopy study of the chemical state of “invisible” Au in synthetic minerals in the Fe-As-S system

ALEXANDER L. TRIGUB<sup>1,2,3</sup>, BORIS R. TAGIROV<sup>1,\*</sup>, KRISTINA O. KVASHNINA<sup>4,5</sup>, DMITRIY A. CHAREEV<sup>1,6,7</sup>, MAXIMILIAN S. NICKOLSKY<sup>1</sup>, ANDREY A. SHIRYAEV<sup>1,8</sup>, NINA N. BARANOVA<sup>9</sup>, ELENA V. KOVALCHUK<sup>1</sup>, AND ANDREY V. MOKHOV<sup>1</sup>

<sup>1</sup>Institute of Geology of Ore Deposits (IGEM RAS), 35, Staromonetnyi per., 119017 Moscow, Russia

<sup>2</sup>National Research Centre “Kurchatov Institute”, 1, Akademika Kurchatova Square, 123182 Moscow, Russia

<sup>3</sup>Physico-Technical Institute of UB RAS, Kirova st. 132, 426000 Izhevsk, Russia

<sup>4</sup>ESRF, The European Synchrotron, CS40220, 38043 Grenoble Cedex 9, France

<sup>5</sup>Helmholtz-Zentrum Dresden-Rossendorf (HZDR), Institute of Resource Ecology, P.O. Box 510119, 01314, Dresden, Germany

<sup>6</sup>Institute of Experimental Mineralogy (IEM RAS), 142432 Chernogolovka, Moscow Region, Russia

<sup>7</sup>Institute of Physics and Technology, Ural Federal University, Mira st., 19, 620002 Ekaterinburg, Russia

<sup>8</sup>Institute of Physical Chemistry and Electrochemistry (IPCE RAS), 31 korp. 4, Leninsky Prospect, 119071 Moscow, Russia

<sup>9</sup>Vernadsky Institute of Geochemistry and Analytical Chemistry (GEOKHI RAS), 19, Kosygina str., 119991 Moscow, Russia

### ABSTRACT

Minerals of the Fe-As-S system are the main components of Au ores in many hydrothermal deposits, including Carlin-type Au deposits, volcanogenic massive sulfide deposits, epithermal, mesothermal, sedimentary-hosted systems, and Archean Au lodes. The “invisible” (or refractory) form of Au is present in all types of hydrothermal ores and often predominates. Knowledge of the chemical state of “invisible” Au (local atomic environment/structural position, electronic structure, and oxidation state) is crucial for understanding the conditions of ore formation and necessary for the physical-chemical modeling of hydrothermal Au mineralization. In addition, it will help to improve the technologies of ore processing and Au extraction. Here we report an investigation of the chemical state of “invisible” Au in synthetic analogs of natural minerals (As-free pyrite FeS<sub>2</sub>, arsenopyrite FeAsS, and löllingite FeAs<sub>2</sub>). The compounds were synthesized by means of hydrothermal (pyrite) and salt flux techniques (in each case) and studied by X-ray absorption fine structure (XAFS) spectroscopy in a high-energy resolution fluorescence detection (HERFD) mode in combination with first-principles quantum chemical calculations. The content of “invisible” Au in the synthesized löllingite (800 ± 300 ppm) was much higher than that in arsenopyrite (23 ± 14 ppm). The lowest Au content was observed in zonal pyrite crystals synthesized in a salt flux. High “invisible” Au contents were observed in hydrothermal pyrite (40–90 ppm), which implies that this mineral can efficiently scavenge Au even in As-free systems. The Au content of the hydrothermal pyrite is independent of sulfur fugacity and probably corresponds to the maximum Au solubility at the experimental *P-T* parameters (450 °C, 1 kbar). It is shown that Au replaces Fe in the structures of löllingite, arsenopyrite, and hydrothermal pyrite. The Au-ligand distance increases by 0.14 Å (pyrite), 0.16 Å (löllingite), and 0.23 Å (As), 0.13 Å (S) (arsenopyrite) relative to the Fe-ligand distance in pure compounds. Distortions of the atomic structures are localized around Au atoms and disappear at *R* > ~4 Å. Chemically bound Au occurs only in hydrothermal pyrite, whereas pyrite synthesized without hydrothermal fluid contains only Au<sup>0</sup>. The heating (metamorphism) of hydrothermal pyrite results in the decomposition of chemically bound Au and formation of Au<sup>0</sup> nuggets, which coarsen with increasing temperature. Depending on the chemical composition of the host mineral, Au can play a role of either a cation or an anion: the Bader atomic partial charge of Au decreases in the order pyrite (+0.4 e) > arsenopyrite (0) > löllingite (–0.4 e). Our results suggest that other noble metals (platinum group elements, Ag) can form a chemically bound refractory admixture in base metal sulfides/chalcogenides. The content of chemically bound noble metals can vary depending on the composition of the host mineral and ore history.

**Keywords:** Invisible gold, pyrite, arsenopyrite, löllingite, synthetic minerals, X-ray absorption spectroscopy, atomic charges

### INTRODUCTION

Minerals of the Fe-As-S system (pyrite FeS<sub>2</sub>, arsenopyrite FeAsS, and löllingite FeAs<sub>2</sub>) are ubiquitous in sulfide ores in many geologic environments and Au-bearing ore deposits,

including Carlin-type Au deposits (for example, Palenik et al. 2004, and reference therein), volcanogenic massive sulfide (VMS) deposits (e.g., Mercier-Langevin et al. 2011; Vikentyev 2015a), mesothermal (Genkin et al. 1998), epithermal (e.g., Cook et al. 2009), sedimentary-hosted systems (Large et al. 2007), and Archean Au lodes (Goldfarb et al. 2005). These occurrences are an important source of Au, and many of them

\* E-mail: boris1t@yandex.ru

belong to world-class gold deposits (>100 t Au, cf. Genkin et al. 1998; Mercier–Langevin et al. 2011). In these ores Au exists (1) as discrete minerals—compounds with chalcogens (S, Se, Te), semimetals (As, Sb, Bi), or intermetallic compounds with Cu, Ag, Hg, etc.; and (2) in an “invisible” (or refractory) state. “Invisible” Au includes nanoscale particles and Au solid solutions. Neither form can be identified by conventional optical or scanning electron microscopy. Visible nuggets of Au and Au-alloys can be extracted from the ore using, for example, cyanide leaching, whereas “invisible” Au cannot be extracted by conventional ore processing methods. In many deposits the proportion of “invisible” Au can be very high. For example, it reaches 85% at the Uchaly VMS deposit in the South Urals, Russia. The estimated total loss of Au from all VMS deposits of the South Urals region is 10–15 t per year (Vikentyev 2015a).

In hydrothermal ores, pyrite often shows the maximal concentrations of “invisible” Au. In many cases, there is a positive correlation between Au and As in pyrite (e.g., Reich et al. 2005; Deditius et al. 2014), although deposits with Au-rich and As-poor pyrite are also known. For example, colloform pyrite bands and veinlets in the large Agua Rica Cu (Mo–Au) deposit (Argentina) are As-poor (<30 ppm) but contain up to 6.7 ppm Au (Franchini et al. 2015). Several studies of Au-bearing deposits of the Urals (Russia), including VMS deposits (Vikentyev 2015a, 2015b), Novogodnee-Monto Fe–Au-skarn deposit (Ivanova et al. 2015), and Svetlinsk Au–Te deposit (Vikent’eva and Bortnikov 2015), did not reveal any significant correlation between Au and As in pyrite. Hence, depending on the deposit type and ore formation conditions, both As-rich and As-poor pyrites can bear economic Au content, although the highest Au contents were documented in arsenian pyrites.

The understanding of the chemical state of “invisible” Au in sulfide ores is necessary for the physical-chemical modeling of hydrothermal Au mineralization and has important implications for the mineral processing industry. The chemical state of “invisible” Au, including its local atomic environment, position in the host mineral structure in the case of solid solution, and valence state can be reliably determined only by spectroscopic methods. Previously, Au-bearing sulfides were studied by X-ray photoelectron (XPS, see Widler and Seward 2002 and reference therein; Laptev and Rozov 2006), Mössbauer (Cardile et al. 1993; Genkin et al. 1998; Kozerenko et al. 2001), and X-ray absorption near edge structure (XANES) spectroscopy (Simon et al. 1999; Cabri et al. 2000). Our study aims at determining the chemical state of “invisible” Au in pyrite, arsenopyrite, and löllingite (FeAs<sub>2</sub>) by X-ray absorption spectroscopy (XAS) in a high-energy resolution fluorescence detection mode (HERFD), with emphasis on Au solid solution. To estimate the conditions favoring formation of this form of “invisible” Au, we synthesized Au-bearing chalcogenides using different methods (hydrothermal and salt flux) at contrasting  $T/f_{S_2}$  conditions, characterized the amount and distribution of Au, and determined the local environment of Au using XAS. An in situ heating experiment was performed to estimate the effect of metamorphism on chemically bound Au in pyrite. The experimental data were combined with first-principles quantum chemical calculations and Bader charge analysis to reveal the local atomic environment and oxidation state of Au in pyrite, arsenopyrite, and löllingite.

## METHODS

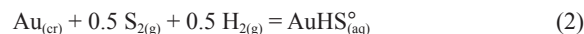
Complete details on the methods are found online<sup>1</sup>, including the synthesis experiments, analytical methods, XAS measurements and data processing, DFT calculations, and XANES spectra simulation.

## RESULTS

### Au content and distribution in synthesized minerals

**Pyrite FeS<sub>2</sub>.** The contents of Au in the hydrothermal pyrites and coexisting aqueous fluid (450 °C, 1 kbar) are presented in Supplemental<sup>1</sup> Table S1. The hydrothermal pyrite is a fine-grained aggregate of particles <10 μm in size (Fig. 1a). The powder is free of metallic Au and, therefore, the total Au content determined by the dissolution of the pyrite samples corresponds to “invisible” Au. We note here that the synthesis of pyrite free of metallic Au inclusions was possible only in acidic solutions with a low concentration of dissolved Au. Our attempts to increase the content of “invisible” Au in pyrite using weakly alkaline solutions with high aqueous Au concentrations (up to 0.1 mol × kg H<sub>2</sub>O<sup>-1</sup>, or 2 × 10<sup>5</sup> ppm) yielded a mixture of pyrite and Au metal (Supplemental<sup>1</sup> Fig. S1). The content of Au in pure FeS<sub>2</sub> grains obtained in these experiments was close to the EPMA detection limit of 100 ppm.

Sulfur fugacity was buffered in the hydrothermal experiments owing to elemental sulfur dissolution and hydrolysis reactions (see Supplemental Methods<sup>1</sup>). The concentration of Au in aqueous fluid increases with increasing  $f_{S_2}$  (Fig. 1b). The slope of the linear fit of the experimental Au solubility vs.  $f_{S_2(g)}$  is  $S = 0.67$  in the logarithmic scale. This means that AuHS<sub>(aq)</sub><sup>o</sup> dominates aqueous Au speciation. For this complex  $S = 0.5$ , which is consistent with the reaction



because  $f_{H_2(g)}$  is the same for all experimental points (except for the S+H<sub>2</sub>SO<sub>4</sub> experiment). The observed increase of the slope could be caused by the presence of Au(HS)<sub>2</sub><sup>-</sup> and/or uncertainty of the calculated  $f_{S_2(g)}$  values.

The effect of  $f_{S_2(g)}$  on the content (solubility) of Au in solid sulfide determines the stoichiometry of the solubility reaction (number of S<sub>2</sub> molecules interacting with Au to form Au-bearing sulfide)



and, therefore, the Au/S ratio and the formal oxidation state of Au in the sulfide. In contrast to the Au solubility in aqueous fluid, the content of Au in hydrothermal pyrite is weakly sensitive to  $f_{S_2}$  and oxidation potential and always falls within the 40–90 ppm range (Supplemental<sup>1</sup> Table S1). We consider a value of ~100 ppm as an upper Au concentration limit for the  $T$ - $P$  conditions of the synthesis experiments. Formally, the slope  $S \sim 0$  may indicate that Au does not interact with dissolved sulfur and, therefore, the Au oxidation state in the sulfide remains unchanged. However, the real structural position and valence state of Au distributed in the

<sup>1</sup>Deposit item AM-17-55832, Supplemental Materials. Deposit items are free to all readers and found on the MSA web site, via the specific issue’s Table of Contents (go to [http://www.minsocam.org/MSA/AmMin/TOC/2017/May2017\\_data/May2017\\_data.html](http://www.minsocam.org/MSA/AmMin/TOC/2017/May2017_data/May2017_data.html)).

sulfide mineral matrix could be determined only by spectroscopic experiments described in the following section.

Grains of high-temperature pyrite synthesized at 620 °C using the salt flux method show zonal Au distribution with  $C(\text{Au})$  ranging from the LA-ICP-MS detection limit to several hundred parts per million (Supplemental<sup>1</sup> Table S2). The smooth character of the Au time-resolved LA-ICP-MS spectra (Supplemental<sup>1</sup> Fig. S2) suggests that microscopic and submicroscopic inclusions of Au are absent. It is interesting that, in addition to Au, this pyrite sample contains several parts per million Pt, which was accidentally introduced into the charge.

**Arsenopyrite  $\text{FeAsS}$  and löllingite  $\text{FeAs}_2$ .** Examples of arsenopyrite and löllingite crystals are shown in Supplemental<sup>1</sup> Figs. S3 and S4, respectively. Two types of LA-ICP-MS spectra were obtained for the arsenopyrite. The first type shows Au-rich (hundreds of parts per million) and Au-poor (up to 30 ppm) zones (top of Supplemental<sup>1</sup> Fig. S5), and the second type corresponds to homogeneously distributed Au at  $C(\text{Au}) \sim 10 \div 30$  ppm (Supplemental<sup>1</sup> Fig. S5, bottom). In the löllingite Au is distributed homogeneously at  $C(\text{Au}) = 800 \pm 300$  ppm (Supplemental<sup>1</sup> Fig. S6).

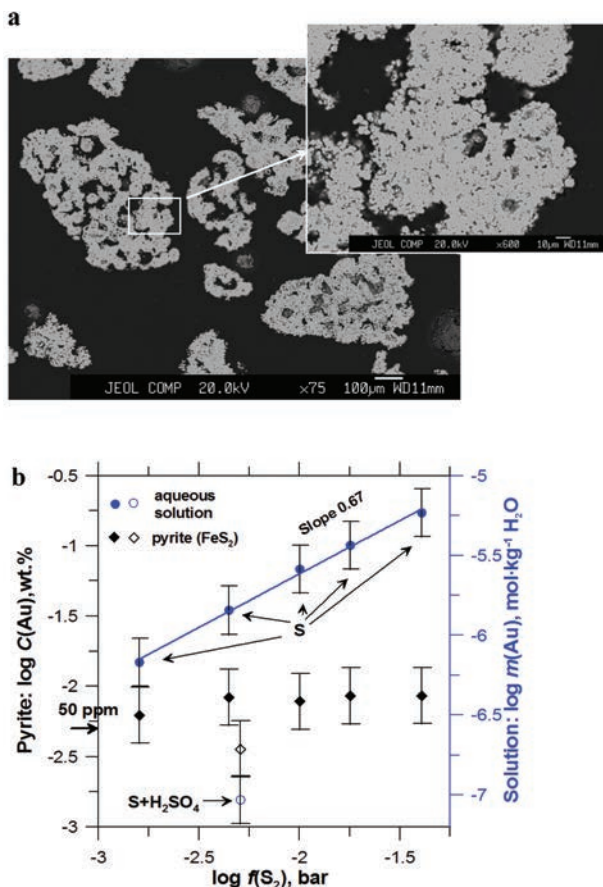


**FIGURE 1.** Results of the pyrite hydrothermal synthesis experiment,  $T = 450$  °C,  $P = 1$  kbar. (a) BSE image of the fine-grained aggregate of the synthetic pyrite; (b) the concentration of Au in pyrite and coexisting aqueous fluid as a function of sulfur fugacity. Filled symbols = sulfur was used to control  $f_{\text{S}_2}$ ; empty symbols correspond to the S+H<sub>2</sub>SO<sub>4</sub> system (last row in Supplemental<sup>1</sup> Table S1), where  $f_{\text{S}_2}$  value has to be corrected. (Color online.)

## XANES spectroscopy

**Ambient-temperature experiment.** The HERFD-XANES spectroscopic technique could be used to acquire Au  $L_3$ -edge spectra not only for pyrite but also for arsenopyrite and löllingite, in which the signal from the trace amount of "invisible" Au is masked by the As  $K$ -edge in the TFY mode (Fig. 2). Another advantage of this technique is that the weak features of Au(I) spectra are considerably enhanced compared with TFY spectra, which facilitates interpretation and modeling. Figure 3a shows Au  $L_3$ -edge HERFD-XANES spectra of Au-bearing pyrite (hydrothermal), arsenopyrite, and löllingite together with spectra of model substances. All these minerals contain Au in the chemically bound state that is different from both Au<sub>(cr)</sub> and Au<sub>2</sub>S. The positions of the edge jump (e.j.) and the first intense feature (white line, WL) are given in Table 1. We observed a significant positive energy shift of the e.j. position increasing in the order pyrite < arsenopyrite < löllingite. A positive e.j. shift usually indicates an increase in the positive charge of the excited atom. However, we will show below that this is not the case for the Fe-As-S system.

The Au  $L_3$ -edge absorption is related to  $2p-5d$  dipole-allowed transitions:  $2p_{3/2} \rightarrow 5d_{5/2}/5d_{3/2}$ . Therefore, the WL intensity reflects the number of empty states in the  $5d_{5/2}$  and  $5d_{3/2}$  orbitals above the Fermi level. The WL intensity for arsenopyrite and löllingite is much greater than that for pyrite (Fig. 3a), indicating a higher number of holes in the  $5d$  electronic shell of As-bearing minerals. Another important characteristic of the Au  $L_3$ -edge HERFD-XANES spectra of these minerals is the negative correlation between the intensity of the second feature at  $\sim 11929$  eV and As content. This can be clearly seen in the spectra of Au-bearing pyrite, the arsenopyrite spectra contain only traces of the feature, and it is absent in the löllingite spectra.

A comparison of the spectra of arsenopyrite and löllingite with those of synthetic AuSb<sub>2</sub> and Au<sub>2</sub>Bi revealed a significant positive shift of the e.j. position increasing in the order Au<sub>2</sub>Bi < AuSb<sub>2</sub> < Au in arsenopyrite < Au in löllingite (Fig. 3b, Table 1).

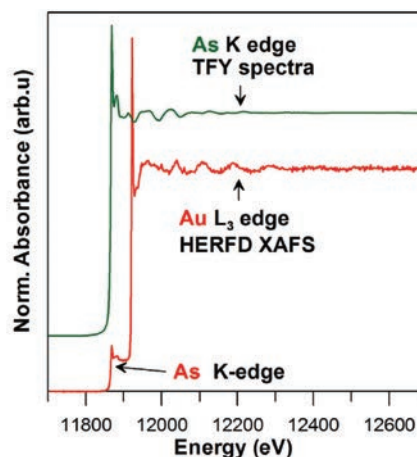


**FIGURE 2.** Difference between the TFY and HERFD spectra for the löllingite sample,  $C(\text{Au}) = 800$  ppm. In TFY mode, the Au features are completely masked by the As  $K$ -edge. The HERFD mode makes it possible to record the Au  $L_3$ -edge spectra. (Color online.)

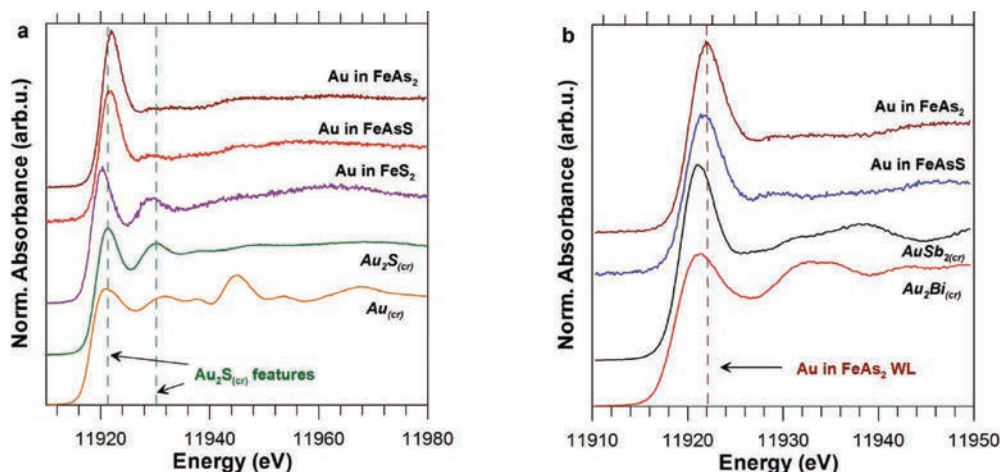


**FIGURE 3.** The Au  $L_3$ -edge HERFD-XANES spectra of the Au-bearing pyrite (hydrothermal synthesis, sample 6-16), arsenopyrite, löllingite (salt flux synthesis), and model substances. (a) Comparison with  $Au_{(cr)}$  and  $Au_2S_{(cr)}$ ; (b) enlarged energy scale, a comparison of arsenopyrite and löllingite with  $AuSb_2$  and  $Au_2Bi$ . Note that the spectra of all the samples of hydrothermal pyrites shown in Figure 1 were similar to the spectra of sample 6-16 shown in this figure. (Color online.)

**TABLE 1.** Position of edge jump (e.j.) and white line (WL) of Au  $L_3$ -edge HERFD-XANES spectra

Sample/Standard	Feature	Position, eV
Löllingite $FeAs_2$	e.j.	11920.1
	WL	11922.0
Arsenopyrite $FeAsS$	e.j.	11919.7
	WL	11921.5
Hydrothermal pyrite $FeS_2$	e.j.	11918.6
	WL	11920.3
$AuSb_2$	e.j.	11919.4
	WL	11920.0
$Au_2Bi$	e.j.	11918.6
	WL	11921.2
$Au_2S$	e.j.	11919.0
	WL	11921.3
Au metal	e.j.	11918.1
	WL	11921.1

Note: Uncertainty is  $\pm 0.2$  eV.

This order corresponds to a decrease in the number of the chemical element in the 15th group of the periodic system and implies that Au is chemically bound to As in the arsenopyrite and löllingite matrices.

**Pyrite heating experiment.** This experiment (Fig. 4) was aimed at modeling the behavior of chemically bound “invisible” Au during hydrothermal ore metamorphism. The spectra collected at ambient temperature indicate different chemical states of Au in hydrothermal and salt flux pyrites. Chemically bound “invisible” Au exists only in the hydrothermal pyrite. Well-crystallized large pyrite grains formed in the eutectic anhydrous chloride mixture contain mostly metallic  $Au^0$ . Heating of the hydrothermal pyrite to 460 °C results in the decomposition of the Au-bearing phase and precipitation of  $Au^0$ . Note that this process takes place even in the presence of  $S_{(liq)}$ , which should promote the formation of an Au-bearing solid solution (Eq. 3). Further heating to 630 °C results in a dramatic drop of the XAFS signal; the spectrum collected at this temperature indicates traces of chemically bound Au. This can be explained by the coalescence of Au nanoparticles. These data are consistent with the analyses of natural Au-bearing arsenopyrite reported by

Wagner et al. (2007), which showed that metamorphism caused Au depletion in arsenopyrite. The irreversible coarsening of Au nanoparticle during arsenian pyrite heating was observed by means of in situ transmission electron microscopy (Reich et al. 2006). Our results demonstrate that the heating (metamorphism) of Au-bearing pyrite results in the decomposition of chemically bound “invisible” Au incorporated into the hydrothermal pyrite matrix during ore formation.

### EXAFS analysis

The EXAFS spectra of pyrite and löllingite are shown in Figure 5. Contamination with metallic Au hampered the collection of good quality EXAFS spectra for arsenopyrite; therefore, only the XANES region was used to characterize the chemical state of Au in this mineral. The EXAFS spectra of pyrite and löllingite (Fig. 5, top) are different: the maxima of the EXAFS function of the latter are clearly shifted to higher  $k$  values. The main peak in the Fourier transforms (FTs) of the löllingite EXAFS function (Fig. 5, bottom) lies at higher  $R$  values, reflecting a larger Au-L distance in the first coordination shell. The results of the least-squares fit of the FTs are shown by thick red lines in Figure 5, and the calculated model parameters are given in Table 2. For both minerals, the best fit of the experimental spectra is achieved for Au occupying the position of Fe in the mineral structure. In these minerals (see Supplemental<sup>1</sup> Structures), the metal atom is octahedrally coordinated. In the structure of pyrite, the first neighbors of Au are 6 S atoms at 2.40 Å distance; in the structure of löllingite, 6 As atoms at 2.52 Å. Due to the large Au ionic radius, the Au-L distances increase by 0.14 and 0.16 Å relative to the crystal structures of pure pyrite and löllingite. Fitting of the first coordination shell of Au yielded  $N = 5.9 \pm 1.5$  and  $5.3 \pm 0.8$  for pyrite and löllingite, respectively, confirming the octahedral coordination of Au in these minerals. The distortion of the local environment around Au in pyrite decreases to 0.06–0.08 Å for S atoms in the second coordination shell, and the Au-Fe distance

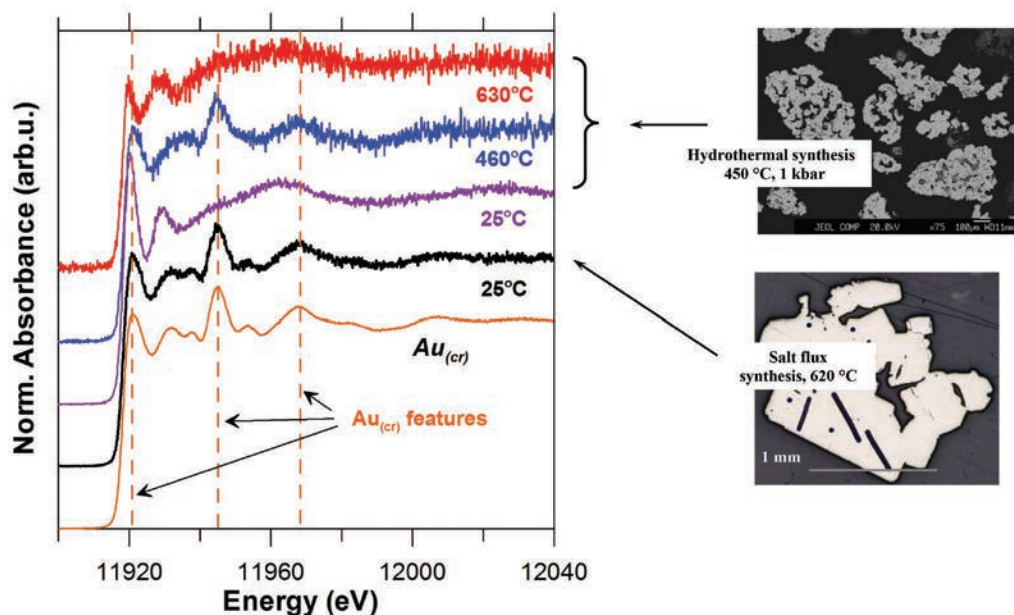


FIGURE 4. The Au  $L_{3}$ -edge HERFD-XANES spectra of pyrites synthesized using the hydrothermal [sample 6-16,  $C(\text{Au}) = 36$  ppm] and salt flux techniques [CD-624,  $C(\text{Au}) \sim 60$  ppm, measured concentrations of Au in this sample are listed in Supplemental Table S2]. The heating of hydrothermal pyrite resulted in a decomposition of the chemically bound Au and a decrease in signal intensity. At 630 °C, the spectra corresponded to the traces of the chemically bound Au whose concentration continuously decreased with time during the experiment (see text for explanation). Vertical lines indicate the position of the three main features of  $\text{Au}_{(\text{cr})}$ . (Color online.)

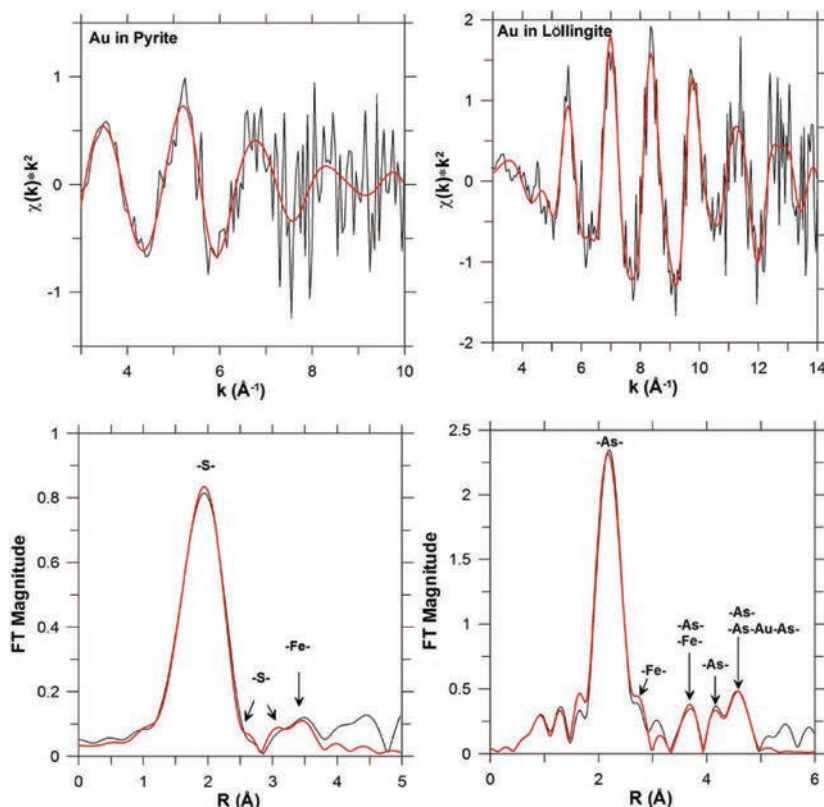


FIGURE 5. EXAFS spectra of Au-bearing pyrite (left panel, hydrothermal synthesis) and löllingite (right panel, salt flux synthesis). (top) Background subtracted EXAFS spectra,  $k^2$  weighted; (bottom) Fourier transforms of the  $k^2$  weighted EXAFS spectra, not corrected for phase shift. Paths are indicated near the FT features. Thin black lines = experiment, thick red lines = fit results. (Color online.)

**TABLE 2.** Au local atomic structure in pyrite and löllingite determined by EXAFS fitting and DFT calculations

Bond	EXAFS N	R, Å	$\sigma^2$ , Å <sup>-2</sup>	E <sup>0</sup> , eV	Fit quality, R-factor	Quantum Espresso R, Å	Crystal structure <sup>a</sup>
<b>Au in pyrite</b>							
Au-S	6	2.40 ± 0.028	0.014 ± 0.0014	6.4 ± 3.5	0.005	2.455	2.264
Au-S	6	3.51 ± 0.16	0.027 ± 0.024			3.499	3.445
Au-S	2	3.69 ± 0.11	0.008 ± 0.018			3.854	3.613
Au-Fe	12	3.79 ± 0.19	0.034 ± 0.023			3.577	3.830
<b>Au in löllingite</b>							
Au-As	6	2.52 ± 0.007	0.005 ± 0.00003	1.2 ± 1.9	0.011	2.536	2.361
Au-Fe	2	3.00 ± 0.025	0.006 ± 0.002			2.973	2.882
Au-As	4	3.88 ± 0.032	0.006 ± 0.004			3.739	3.726
Au-As	6	4.06 ± 0.056	0.006 ± 0.004			3.984	3.927
Au-Fe	8	4.23 ± 0.032	0.008 ± 0.007			4.261	4.249
Au-As	4	4.67 ± 0.054	0.004 ± 0.010			4.737	4.723
Au-As	6	4.82 ± 0.058	0.004 ± 0.010			4.869	4.871

Notes: The last column shows interatomic distances for the unrelaxed structure of pure minerals. Uncertainties are calculated by the Artemis code.

<sup>a</sup> Unrelaxed structures: Bayliss (1977) for pyrite and Lutz et al. (1987) for löllingite.

for the nearest Fe atoms at ~3.8 Å remains almost unchanged (within 0.04 Å). Similar relations are observed for löllingite: the distortion of the crystalline structure decreases for distant coordination shells and disappears at  $R > 4.2$  Å.

### DFT calculations

Interatomic distances optimized by the DFT method for pyrite and löllingite are given in Table 2. In the case of löllingite, good agreement is observed between the simulated structure and the results of the EXAFS spectra fitting for the first and second neighbors ( $\pm 0.02$  Å for the first coordination shell at 2.5 Å and  $\pm 0.03$  Å for the second shell at 3 Å). Similar results were obtained in our recent study of Au-bearing covellite CuS, the EXAFS model of which was adequately reproduced by DFT simulation at distances up to 4 Å (agreement between DFT calculations and EXAFS fitting was within 0.01–0.04 Å depending on the distance) (Tagirov et al. 2016). Based on these results, we can suggest that our method of DFT calculation reproduces the atomic coordinates of Au-bearing chalcogenides within  $\pm 0.02$  and 0.04 Å, at least for the first two coordination shells located at distances up to 3 Å.

In the case of pyrite, the agreement between the DFT simulation and EXAFS fit is poor: the difference is 0.055 Å for the first neighbors around Au atom. This fact can be explained by the thermodynamic instability of Au-bearing pyrite, the structure of which cannot be accurately reproduced by equilibrium structure relaxation methods. This inference is consistent with the results of the pyrite heating experiment, in which chemically bound Au was decomposed at high temperature and escaped from the FeS<sub>2</sub> matrix. This is opposite to the general rule that an increase in temperature tends to stabilize solid solutions.

Table 3 reports the results of the DFT simulation of the local atomic environment of Au-bearing arsenopyrite. The distances

**TABLE 3.** Au local atomic structure in arsenopyrite determined by DFT calculations compared to the unrelaxed structure of pure arsenopyrite

Bond	N	Quantum Espresso R, Å	Crystal structure <sup>a</sup> R, Å
Au-S	3	2.466	2.231
Au-As	3	2.530	2.397
Au-Fe	2	2.984; 3.655	2.734; 3.741
Au-S	4	3.719; 3.739; 3.779; 3.781	3.681; 3.725; 3.762; 3.762
Au-As	4	3.791; 3.811; 3.913; 3.919	3.693; 3.3.755; 3.755; 3.798

<sup>a</sup> Unrelaxed structure from Bindi et al. (2012).

Au-S and Au-As in the first coordination shell increase by 0.13 and 0.23 Å, respectively. The Au-Fe distance for the nearest two Fe atoms increases by 0.25 Å relative to pure arsenopyrite. This model was checked by the results of Au L<sub>3</sub>-edge HERFD-XANES spectra simulation, which is described below.

### XANES spectra simulation

The results of Au L<sub>3</sub>-edge HERFD-XANES spectra modeling are shown in Figures 6a–6c. The FDMNES simulation of Au in pyrite spectrum (Fig. 6a) overestimates the WL intensity and shifts the second feature by ~–2 eV relative to the experimental spectrum. This disagreement probably stems from the metastable nature of “invisible” Au in pyrite, which leads to discrepancies in FDM SCF-based spectra modeling. The spectrum calculated using the FEFF9 computer code is given for comparison. The agreement between the experimental and simulated spectra is good, with the exception of the third diffuse feature with a centroid at ~11 945 eV, which is absent in the calculated spectrum.

The simulated spectrum of löllingite is in good agreement with the experimental one (Fig. 6b). The only difference is the overestimated width of WL. The intensity and positions of the spectral features for Au-bearing arsenopyrite are correctly reproduced by the FDMNES calculation (Fig. 6c), which supports our results of DFT calculation for this mineral.

Theoretical FDMNES calculations showed that the second feature in the spectra of Au bearing pyrite and arsenopyrite (at ~11 929 eV) originates mostly from the mixing of hybridized Au *p*, *d* and S *p* orbitals. At this energy, the contribution of As *p* empty valence states to chemical bond formation is weak for arsenopyrite and negligible for löllingite. This is why the second feature is intense in the spectra of Au-bearing pyrite and absent in the löllingite spectra.

Despite the fact that both the FDMNES and FEFF programs calculate charge states using the muffin-tin approximation, the FEFF code is known to be more efficient for systems with isotropic potential compared with systems with anisotropic potential, whereas the FDMNES program successfully reproduces charge states and spectral features in systems of both types. The fact that the theoretical spectra of Au-bearing pyrite obtained by the FEFF code are in close agreement with the experimental Au L<sub>3</sub>-edge XANES is indicative of a highly symmetric environment (octahedral) of Au in pyrite, rather than a linear coordination like that in Au<sub>2</sub>S.

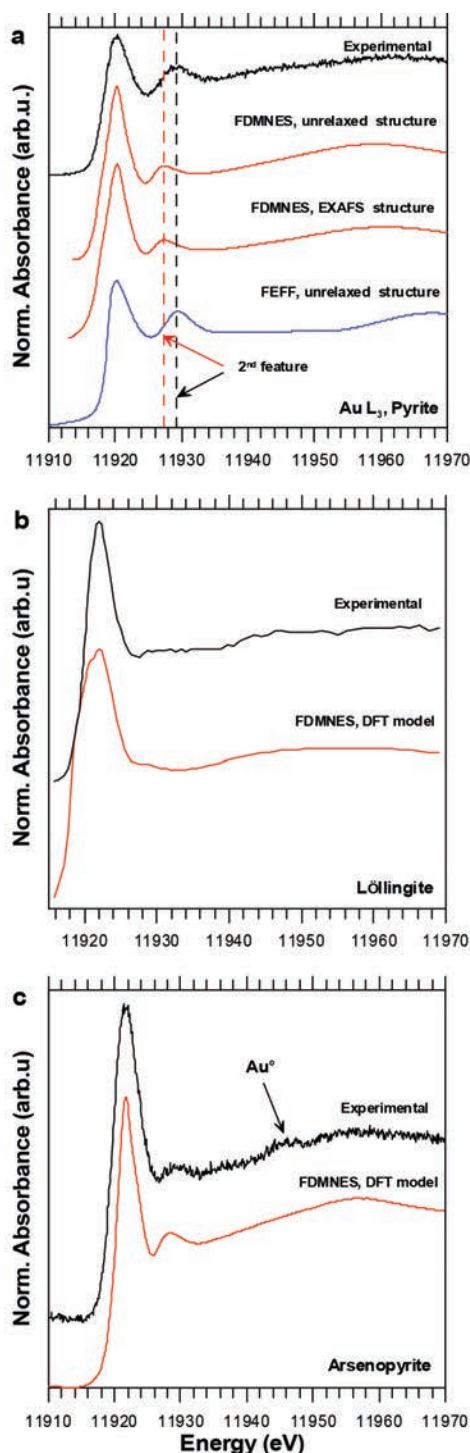


**FIGURE 6.** Results of a theoretical calculation of Au  $L_3$ -edge HERFD-XANES spectra for Au-bearing pyrite (a), löllingite (b), and arsenopyrite (c). Experimental spectra are shown for comparison [pyrite: sample 6-16, hydrothermal,  $C(\text{Au}) = 36$  ppm; löllingite: sample 5333, salt flux synthesis,  $C(\text{Au}) = 800 \pm 300$  ppm; arsenopyrite: sample 5140, salt flux synthesis,  $C(\text{Au}) = 23 \pm 14$  ppm]. For pyrite, the EXAFS structure was built by setting the first-neighbor Au-S distances in accordance with the EXAFS model (Table 2), whereas all the other distances were adopted from the unrelaxed structure of pure pyrite. (Color online.)

### The valence state of “invisible” Au

The results of the Bader analysis of electron density performed using QTAIM for the pure and Au-bearing minerals are summarized in Supplemental Table S3. The partial atomic charge of S in pyrite is more negative than that of As in löllingite ( $-0.7$  e for disulfide group in pyrite vs.  $-0.08$  e for As in löllingite). The topological charge of As in arsenopyrite is  $+0.18$  e, whereas S is negatively charged ( $-0.6$  e). These atomic partial charges reflect the distribution of delocalized electrons and are in line with Pauling electronegativity:  $\chi(\text{S}) = 2.58 \gg \chi(\text{As}) = 2.18$  (Huheey et al. 2000). In the Au-bearing minerals discussed here, the atomic charge of Au increases in the order löllingite < arsenopyrite < pyrite. Au is positively charged in the pyrite, nearly neutral in the arsenopyrite, and negatively charged in the löllingite. Note that the charge of Au in the löllingite is much more negative than that of As. This is explained by the fact that Au is the most electronegative metal [ $\chi(\text{Au}) = 2.54$ ] whose electron affinity is higher than that of semi-metals.

### DISCUSSION AND IMPLICATIONS

The results of our study demonstrate that Au substitutes for Fe in the crystal structures of pyrite, arsenopyrite, and löllingite. However, the chemical nature of “invisible” Au in these minerals is different. In pyrite, chemically bound Au is formed only in the presence of hydrothermal solution. This is consistent with the results of Widler and Seward (2002) on Au adsorption by pyrite. They found that Au can be efficiently scavenged by natural and synthetic pyrites from acidic aqueous solutions in which  $\text{AuHS}_{(\text{aq})}^0$  is the dominant Au complex. Similar Au adsorption isotherms were observed for  $\text{As}_2\text{S}_3$  and  $\text{Sb}_2\text{S}_3$  by Renders and Seward (1989). In view of these results, our observation of independence of Au concentration in pyrite on  $f_{\text{S}_2}$  (and, consequently, on  $\text{AuHS}_{(\text{aq})}^0$  concentration) can be attributed to the attainment of the maximum pyrite sorption capacity with respect to Au. In contrast, pyrite grains synthesized in a dry salt melt contain only  $\text{Au}^0$ . Furthermore, heating of hydrothermal pyrite in a dry system results in the decomposition of chemically bound Au.

The XPS measurements by Widler and Seward (2002) on Au-bearing pyrites showed that the chemical state of Au in pyrite is different from  $\text{Au}^0$ . The Au  $4f_{7/2}$  electron binding energy (BE) is 84.8 eV for Au in pyrite, whereas  $BE = 84.0$  eV for metallic Au. A similar value of  $BE = 85.1$  eV was obtained for Au-bearing pyrite synthesized at 200 °C (Laptev and Rozov 2006). This value is higher than Au  $4f_{7/2}$  BE in  $\text{Au}_2\text{S}$ , where Au is linearly coordinated with two S atoms ( $BE_{\text{Au}/\text{Au}_2\text{S}} \sim 84$  eV, Tagirov et al. 2014) implying different local environments of Au in pyrite and  $\text{Au}_2\text{S}$ . However, the core level XPS technique is less sensitive to local atomic environment geometry and chemical bonding compared to XAFS spectroscopy, which is appropriate for reliable determination of the chemical state of Au.

The present study and experimental investigations of Au-bearing As-free pyrites (Fadeev and Kozerenko 1999; Kozerenko et al. 2001; Widler and Seward 2002; Laptev and Rozov 2006) combined with data on Au contents in sulfide ores from different geologic environments, suggest that pyrite can efficiently uptake Au even in As-poor systems, if large amounts of hydrothermal ore are rapidly formed. Such a process may occur, for example, in hydrothermal black smoker systems where fine-grained

sulfides are formed owing to the mixing of hydrothermal solutions with cold oxidized seawater (Bortnikov et al. 2003; Grichuk 2012). The content of chemically bound "invisible" Au in As-free pyrite determined in the present study for 450° (tens of parts per million) is somewhat lower than the maximum values of ~100 ppm measured in pyrite synthesized at 200 °C (Laptev and Rozov 2006) and ~100–300 ppm in the ambient-temperature sorption experiments of Widler and Seward (2002). Neglecting differences in surface area or grain size, which is usually within  $1+n \times 10 \mu\text{m}$  for fine-grained pyrite, the maximum content of chemically bound Au in As-free hydrothermal pyrite formed at 25–450 °C can be estimated as  $30 \text{ ppm} < C(\text{Au}) < 300 \text{ ppm}$ . A temperature increase tends to reduce the Au content, which is partly compensated by the stabilization and enrichment of  $\text{AuHS}_{(\text{aq})}^{\circ}$  in high-temperature solution/fluid (Stefánsson and Seward 2004). The maximum content of chemically bound "invisible" Au in hydrothermal pyrite can be roughly estimated as 100–300 ppm at 25 °C, ~150 ppm at 100 °C, ~100 ppm at 200 °C, and 100–50 ppm at 300–500 °C; a retrograde behavior is thus evident. One should expect that excess Au will be present in the metallic state. This behavior of "invisible" Au in synthetic pyrite is consistent with published data on natural minerals (e.g., Fig. 9a in Deditius et al. 2014).

In contrast to pyrite, Au can form an isomorphous solid solution in arsenopyrite and löllingite even at high temperatures (>500 °C) in the absence of aqueous fluid. This suggests a thermodynamic stability of this form of chemically bound Au in these minerals. The maximum content of chemically bound "invisible" Au is tens parts per million for arsenopyrite and hundreds parts per million for löllingite. Our data are consistent with natural observations, which show that As stabilizes Au-bearing sulfides and leads to an increase in Au content (cf. Reich et al. 2005; Deditius et al. 2014). Further insight into the speciation of chemically bound Au can be drawn from the fact that As substitutes for S in pyrite with formation of an isomorphous solid solution showing significant clustering of As atoms (Zotov et al. 1972; Savage et al. 2000; Reich and Becker 2006). However, more spectroscopic data are necessary to determine unambiguously the chemical state of As and Au in arsenian pyrite.

A comparison of the Au  $L_{3\text{-edge}}$  HERFD-XANES spectra shows that edge energy (e.j.) increases when As replaces S in the order pyrite < arsenopyrite < löllingite (Table 1, Fig. 3a). Usually, the atomic charge increases in the same order, becoming more positive at higher e.j. (higher energy is necessary to excite the core level electron). However, the data in Supplemental<sup>1</sup> Table S3 show that the opposite is true: the Au charge is positive in pyrite and negative in löllingite. Such an e.j. behavior cannot be explained by the effect of the atomic charge alone and needs further examination.

The WL position and intensity indicate that the number of Au  $5d$  unoccupied electronic states increases in As-bearing phases relative to pyrite, despite the fact that Au is more electronegative than As. This peculiarity can be explained by the charge compensation model describing the charge flow in Au alloys (Watson et al. 1971). In this model, the Au  $d$ -charge loss upon alloying is overcompensated by conduction (mainly  $s$ - $p$ ) charge gain from the second alloy component. As a result, Au gains an overall negative charge (see Kuhn and Sham 1994; Bzowski et

al. 1995, and reference therein).

The fact that the valence state of Au can vary depending on the host mineral composition (Supplemental<sup>1</sup> Table S3) demonstrates that coupled charge-compensation substitution is not necessary for the formation of isomorphous solid solutions in crystals with highly covalent chemical bonds.

Along with Au, other noble metals (platinum group elements, Ag) often occur as an "invisible" admixture in sulfide ore (cf. Filimonova et al. 2015, and reference therein). Considering their chemical state in sulfide minerals from the point of view of our study, we suggest that these metals can also form a chemically bound refractory admixture. The chemical state and the concentration of this form of noble metals can vary with the local atomic environment/structural position and valence state depending on the composition of host sulfide and ore origin (e.g., hydrothermal, magmatic, or metamorphic). Further spectroscopic studies, including in situ X-ray absorption/emission spectroscopy at high  $T$ - $P$  parameters, will help to determine the chemical state of noble metals and mechanisms of ore-forming processes.

## ACKNOWLEDGMENTS

The authors acknowledge ESRF for allocating beamtime under proposals ES-184 and ES-360. The help and support of Sara Lafuerza and Pieter Glatzel during the beamtime is greatly appreciated. B.R.T. and K.O.K. thank Hugo Vitoux for outstanding technical support during the in situ experiment with micro-furnace at the ID26 beamline. We are grateful to Sara-J. Barnes for organizing the LA-ICP-MS measurements at the University of Chicoutimi, V. Abramova and E. Minervina for the LA-ICP-MS analysis of synthesized minerals. We are grateful to Andrey Girmis and Anastasia Plyasunova for correction of English grammar. We thank Barbara Etschmann, Martin Reich, and an anonymous reviewer for helpful comments and suggestions. The results of this work were obtained using the computational resources of MCC NRC "Kurchatov Institute" (<http://computing.kiae.ru/>). This study was supported by the Russian Scientific Foundation, grant no. 14-17-00693; RFBR grant no. 16-05-00938 supported salt flux synthesis experiments. D.Ch. was involved in Act 211 Government of the Russian Federation, agreement no. 02.A03.21.0006 (synthesis of sulfides via salt flux technique).

## REFERENCES CITED

- Bayliss, P. (1977) Crystal structure refinement of weakly anisotropic pyrite cubic model. *American Mineralogist*, 62, 1168–1172.
- Bellet, D., Gorges, B., Dallery, A., Bernard, P., Pereiro, E., and Baruchel, J. (2003) A 1300 K furnace for in situ X-ray microtomography. *Journal of Applied Crystallography*, 36, 366–367.
- Bindi, L., Moelo, Y., Leone, P., and Suchaud, M. (2012) Stoichiometric arsenopyrite, FeAsS, from La Roche-Balue Quarry, Loire-Atlantique, France: Crystal structure and Mössbauer study. *Canadian Mineralogist*, 50, 471–479.
- Blöchl, P.E. (1994) Projector augmented-wave method. *Physical Review B*, 50, 17,953–17,979.
- Bortnikov, N.S., Cabri, L.J., Vikentiev, I.V., Tagirov, B.R., Mc Mahon, G., Bogdanov, Yu. A., and Stavrova, O.O. (2003) Invisible gold in sulfides from seafloor massive sulfide edifices. *Geology of Ore Deposits*, 45, 201–212.
- Bunău, O., and Joly, Y. (2009) Self-consistent aspects of X-ray absorption calculations. *Journal of Physics: Condensed Matter*, 21, 345501.
- Bzowski, A., Yiu, Y.M., and Sham, T.K. (1995) Charge redistribution in Au-metalloid intermetallics: A Au  $L_{2,3}$ -edge X-ray absorption study. *Physical Review B*, 51, 9515–9520.
- Cabri, L.J., Newville, M., Gordon, R.A., Daryl Crozier, E., Sutton, S.R., McMahon, G., and Jiang, D.T. (2000) Chemical speciation of gold in arsenopyrite. *Canadian Mineralogist*, 38, 1265–1281.
- Cardile, C.M., Cashion, J.D., McGrath, A.C., Renders, P., and Seward, T.M. (1993) <sup>197</sup>Au Mössbauer study of Au<sub>2</sub>S and gold adsorbed onto As<sub>2</sub>S<sub>3</sub> and Sb<sub>2</sub>S<sub>3</sub> substrates. *Geochimica et Cosmochimica Acta*, 57, 2481–2486.
- Chou, I.-M. (2012) Optical cells with fused silica windows for the study of geological fluids. In J. Dubessy, M.-C. Gaumont, and F. Rull, Eds., *Applications of Raman Spectroscopy to Earth Sciences and Cultural Heritage*, 12, p. 227–248. EMU Notes in Mineralogy, London.
- Chou, I.-M., Song, Y., and Burruss, R.C. (2008) A new method for synthesizing fluid inclusions in fused silica capillaries containing organic and inorganic material. *Geochimica et Cosmochimica Acta*, 72, 5217–5231.
- Cook, N.J., Ciobanu, C.L., and Mao, J. (2009) Textural control on gold distribution in As-free pyrite from the Dongping, Huangtuliang and Hougou gold deposits,

- North China Craton (Hebei Province, China). *Chemical Geology*, 264, 101–121.
- Deditius, A.P., Reich, M., Kesler, S.E., Utsunomiya, S., Chryssoulis, C.L., Walshe, J., and Ewing, R.C. (2014) The coupled geochemistry of Au and As in pyrite from hydrothermal ore deposits. *Geochimica et Cosmochimica Acta*, 140, 644–670.
- Ding, J. (2010) The pH determination of palaeofluids: experimental and thermodynamic approach, 173 p. Ph.D. thesis, Université Henri Poincaré, Nancy.
- Fadeev, V.V., and Kozerenko, S.V. (1999) Gold in processes of pyrite formation. Part 1. Gold accumulation during pyrite formation. *Geochemistry International*, 37, 1182–1190.
- Filimonova, O.N., Minervina, E.A., Kovalchuk, E.A., Abramova, V.D., Vikent'iev, I.V., Tagirov, B.R., Chareev, D.A., and Chvosticov, V.A. (2015) An experimental study of noble and base metals (Au, Ag, Pt, Pd, Zn) distribution in pyrite and pyrrhotite. In A.-S. André-Meyer et al., Eds., *Proceedings of the 13th Biennial SGA Meeting, Mineral Resources in a Sustainable World*, p. 925–927. Nancy, France.
- Franchini, M., McFarlane, C., Maydagán, L., Reich, M., Lentz, D.R., Meinent, L., and Bouchier, V. (2015) Trace metals in pyrite and marcasite from the Agua Rica porphyry-high sulfidation epithermal deposit, Catamarca, Argentina: Textural features and metal zoning at the porphyry to epithermal transition. *Ore Geology Reviews*, 66, 366–387.
- Gauthier, C., Sole, V.A., Signorato, R., Goulon, J., and Moguiline, E. (1999) The ESRF beamline ID26: X-ray absorption on ultra dilute sample. *Journal of Synchrotron Radiation*, 6, 164–166.
- Genkin, A.D., Bortnikov, N.S., Cabri, L.J., Wagner, F.E., Stanley, C.J., Safonov, O.G., McMahon, G., Friedl, J., Kerzin, A.L., and Gamyaniin, G.N. (1998) A multidisciplinary study of invisible gold in arsenopyrite from four mesothermal gold deposits in Siberia, Russian federation. *Economic Geology*, 93, 463–487.
- Giannozzi, P., Baroni, S., Bonini, N., Calandra, M., Car, R., Cavazzoni, C., Ceresoli, D., Chiarotti, G.L., Cococcioni, M., Dabo, I. and others. (2009) QUANTUM ESPRESSO: a modular and open-source software project for quantum simulations of materials. *Journal of Physics: Condensed Matter*, 21, 395502.
- Glattel, P., and Bergman, U. (2005) High resolution 1s core hole X-ray spectroscopy in 3d transition metal complexes—electronic and structural information. *Coordination Chemistry Reviews*, 249, 65–95.
- Goldfarb, R.J., Baker, T., Dube, B., Groves, D.I., Hart, C.J., and Gosselin, P. (2005) Distribution, character, and genesis of gold deposits in metamorphic terranes. *Economic Geology 100th Anniversary Volume*, 407–450.
- Guda, S.A., Guda, A.A., Soldatov, M.A., Lomachenko, K.A., Bugaev, A.L., Lamberti, C., Gawelda, W., Bressler, C., Smolentsev, G., Soldatov, A.V., and Joly, Y. (2015) Optimized finite difference method for the full-potential XANES simulations: application to molecular adsorption geometries in MOFs and metal-ligand intersystem crossing transients. *Journal of Chemical Theory and Computation*, 11, 4512–4521.
- Grichuk, D.V. (2012) Thermodynamic model of ore-forming processes in a submarine island-arc hydrothermal system. *Geochemistry International*, 50, 1069–1100.
- Hedin, L., and Lundqvist, B. (1971) Explicit local exchange-correlation potentials. *Journal of Physics C: Solid State Physics*, 4, 2064–2083.
- Huheey, J.E., Keiter, E.A., and Keiter, R.L. (2000) *Inorganic Chemistry: Principles of structure and reactivity*, 4th ed. Pearson Education.
- Ivanova, Ju.N., Tykova, E.E., Abramova, V.D., Kovalchuk, E.V., and Vikentyev, I.V. (2015) Ores mineralogy and first data about "invisible" form of Au in pyrite of the Novogodnee-Monto deposit (the Polar Urals, Russia). In A.-S. André-Meyer et al., Eds., *Proceedings of the 13th Biennial SGA Meeting, Mineral Resources in a Sustainable World*, p. 121–125. Nancy, France.
- Joly, Y. (2001) X-ray absorption near-edge structure calculations beyond the muffin-tin approximation. *Physical Review B*, 63, 125120.
- Kozerenko, S.V., Wagner, F.E., Friedl, J., and Fadeev, V.V. (2001) Gold in pyrite formation processes: 3. Mössbauer study of synthetic gold-bearing iron sulfides. *Geochemistry International*, 39, Suppl. 2, S167–S172.
- Kresse, G. (1999) From ultrasoft pseudopotentials to the projector augmented-wave method. *Physical Review B*, 59, 1758–1775.
- Kuhn, M., and Sham, T.K. (1994) Charge redistribution and electronic behavior in a series of Au-Cu alloys. *Physical Review B*, 49, 1647–1661.
- Kvashnina, K.O., and Scheinost, A.C. (2016) A Johann-type X-ray emission spectrometer at the Rossendorf Beamline. *Journal of Synchrotron Radiation*, 23, 836–841.
- Laptev, Yu.V., and Rozov, K.B. (2006) Interaction of gold with sulfide surface as a factor of its concentration in hydrothermal ore formation. *Doklady Earth Sciences*, 411, 1229–1232.
- Large, R.R., Maslennikov, V.V., Robert, F., Danyushevsky, L.V., and Chang, Z. (2007) Multistage sedimentary and metamorphic origin of pyrite and gold in the giant Sukhoi Log deposit, Lena Gold Province, Russia. *Economic Geology*, 102, 1233–1267.
- Lutz, H.D., Jung, M., and Wäschchenbach, G. (1987) Kristallstrukturen des löllingits FeAs<sub>2</sub> und des pyrits RuTe<sub>2</sub>. *Zeitschrift für Anorganische und Allgemeine Chemie*, 554, 87–91.
- Mercier-Langevin, P., Hannington, M.D., Dubé, B., and Bécu, V. (2011) The gold content of volcanogenic massive sulfide deposits. *Mineralium Deposita*, 46, 509–539.
- Otero-de-la-Roza, A., Blanco, M.A., Martín Pendás, A., and Luaña, V. (2009) Critic: a new program for the topological analysis of solid-state electron densities. *Computer Physics Communications*, 180, 157–166.
- Otero-de-la-Roza, A., Johnson, E.R., and Luaña, V. (2014) Critic2: A program for real-space analysis of quantum chemical interactions in solids. *Computer Physics Communications*, 185, 1007–1018.
- Palenik, C.S., Utsunomiya, S., Reich, M., Kesler, S.E., Wang, L., and Ewing, R.C. (2004) "Invisible" gold revealed: Direct imaging of gold nanoparticles in a Carlin-type deposit. *American Mineralogist*, 89, 1359–1366.
- Ravel, B., and Newville, M. (2005) ATHENA, ARTEMIS, HEPHAESTUS: data analysis for X-ray absorption spectroscopy using IFEFFIT. *Journal of Synchrotron Radiation*, 12, 537–541.
- Rehr, J.J., Kas, J.J., Vila, F.D., Prange, M.P., and Jorissen, K. (2010) Parameter-free calculations of X-ray spectra with FEFF9. *Physical Chemistry Chemical Physics*, 12, 5503–5513.
- Reich, M., and Becker, U. (2006) First-principles calculations of the thermodynamic mixing properties of arsenic incorporation into pyrite and marcasite. *Chemical Geology*, 225, 278–290.
- Reich, M., Kesler, S., Utsunomiya, S., Palenik, C.S., Chryssoulis, S.L., and Ewing, R.C. (2005) Solubility of gold in arsenian pyrite. *Geochimica et Cosmochimica Acta*, 69, 2781–2796.
- Reich, M., Utsunomiya, S., Kesler, S., Wang, L., Ewing, R.C., and Becker, U. (2006) Thermal behavior of metal nanoparticles in geologic materials. *Geology*, 34, 1033–1036.
- Renders, P.J., and Seward, T.M. (1989) The adsorption of thio gold(I) complexes by amorphous As<sub>2</sub>S<sub>3</sub> and Sb<sub>2</sub>S<sub>3</sub> at 25 and 90 °C. *Geochimica et Cosmochimica Acta*, 53, 255–267.
- Savage, K.S., Tingle, T.N., O'Day, P.A., Waychunas, G.A., and Bird, D.K. (2000) Arsenic speciation in pyrite and secondary weathering phases, Mother Lode Gold District, Tuolumne County, California. *Applied Geochemistry*, 15, 1219–1244.
- Simon, G., Huang, H., Penner-Hahn, J.E., Kesler, S., and Kao, L.S. (1999) Oxidation state of gold and arsenic in gold-bearing arsenian pyrite. *American Mineralogist*, 84, 1071–1079.
- Stefánsson, A., and Seward, T.M. (2004) Gold(I) complexing in aqueous sulphide solutions to 500°C at 500 bar. *Geochimica et Cosmochimica Acta*, 68, 4121–4143.
- Tagirov, B.R., Dikov, Y.P., Buleev, M.I., Koval'chuk, E.V., Chareev, D.A., Kokh, M.A., Borisovskii, S.E., Abramova, V.D., Baranova, N.N., Garas'ko, M.I., and others. (2014) "Invisible" gold in covellite (CuS): synthesis and studies by EPMA, LA-ICP-MS, and XPS techniques. *Doklady Earth Sciences*, 459, Part 1, 1381–1386.
- Tagirov, B.R., Trigub, A.L., Kvashnina, K.O., Shiryayev, A.A., Chareev, D.A., Nickolsky, M.S., Abramova, V.D., and Kovalchuk, E.V. (2016) Covellite CuS as a matrix for "invisible" gold: X-ray spectroscopic study of the chemical state of Cu and Au in synthetic minerals. *Geochimica et Cosmochimica Acta*, 191, 58–69.
- Vikentyev, I.V. (2015a) Invisible and microscopic gold in pyrite: methods and new data for massive sulfide ores of the Urals. *Geology of Ore Deposits*, 57, 237–265.
- (2015b) Invisible and microscopic gold in pyrite: new data for volcanogenic massive sulfide ores of the Urals. In A.-S. André-Meyer et al., Eds., *Proceedings of the 13th Biennial SGA Meeting, Mineral Resources in a Sustainable World*, p. 2113–2116. Nancy, France.
- Vikent'eva, O.V., and Bortnikov, N.S. (2015) The large Svetlinsk Au-Te deposit, South Urals: telluride mineralization for genetic reconstructions. In A.-S. André-Meyer et al., Eds., *Proceedings of the 13th Biennial SGA Meeting, Mineral Resources in a Sustainable World*, 851–854. Nancy, France.
- Wagner, T., Klemm, R., Wenzel, T., and Mattson, B. (2007) Gold upgrading in metamorphosed massive sulfide ore deposits: Direct evidence from laser-ablation-inductively-coupled plasma mass spectrometry of invisible gold. *Geology*, 35, 775–778.
- Watson, R.E., Hudis, J., and Perlman, M.L. (1971) Charge flow and *d* compensation in gold alloys. *Physical Review B*, 4, 4139–4144.
- Widler, A.M., and Seward, T.M. (2002) The adsorption of gold (I) hydrosulphide complexes by iron sulphide surfaces. *Geochimica et Cosmochimica Acta*, 66, 383–402.
- Zabinsky, S.I., Rehr, J.J., Ankudinov, A., Albers, R.C., and Eller, M.J. (1995) Multiple-scattering calculations of X-ray-absorption spectra. *Physical Review B*, 52, 2995–3009.
- Zotov, A.V., Laputina, I.P., and Chichagov, A.V. (1972) Arsenian pyrite from hot springs of Kunashir Island (Kuril Islands). *Geology of Ore Deposits*, No. 1, 125–131 (in Russian).